
Logits of API-Protected LLMs Leak Proprietary Information

Matthew Finlayson Xiang Ren Swabha Swayamdipta
Thomas Lord Department of Computer Science
University of Southern California
{mfinlays, xiangren, swabhas}@usc.edu

Abstract

The commercialization of large language models (LLMs) has led to the common practice of restricting access to proprietary models via an limited API. In this work we show that, with a conservative assumption about the model architecture, it is possible to learn a surprisingly large amount of non-public information about an API-protected LLM from a small number of API queries (e.g., costing under \$1,000 for OpenAI’s `gpt-3.5-turbo`). Our findings are centered on one key observation: most modern LLMs suffer from a softmax bottleneck, which restricts the model outputs to a linear subspace of the full output space. We exploit this fact to unlock several capabilities: efficiently discovering the LLM’s hidden size, obtaining cheap full-vocabulary outputs, detecting and disambiguating different model updates, identifying the source LLM given a single full LLM output, and even estimating the output layer parameters. Our empirical investigations show the effectiveness of our methods, which allow us to estimate the embedding size of OpenAI’s `gpt-3.5-turbo` to be about 4,096. Lastly, we discuss ways that LLM providers can guard against these attacks, as well as how these capabilities can be viewed as a feature (rather than a bug) by allowing for greater transparency and accountability.

1 Introduction

As large language models (LLMs) have become more capable and valuable, it has become increasingly common for companies and organizations to train closed-source LLMs and make them available only via an API [e.g., OpenAI et al., 2024]. This setup may foster a false sense of security for LLM providers, who might mistakenly assume that information about their model architecture is private, and that certain types of attacks on their LLM are infeasible. On the flip side, users must seemingly take providers’ word that LLMs only change when the provider publicly announces version updates.

Despite this apparent state of affairs, in reality many LLM APIs reveal much more information about their underlying models than previously thought. In this paper we show how to extract detailed information about LLM parameterization using only common API configurations. Our findings allow LLM clients to hold providers accountable by tracking model changes, recovering hidden prompts and cheaply obtaining full vocabulary outputs. At the same time, our approach also allows LLM providers to establish unique identities for their models, enabling trust with their users as well as improved accountability. Table 1 summarizes the applications that we explore in this paper.

Our method exploits the low-rank output layer common to most LLM architectures by observing that this layer’s outputs are constrained to a low-dimensional subspace of the full output space, as illustrated in Figure 1. We call this restricted output space the LLM’s *image*. We can obtain a basis for this image by collecting a small number of LLM outputs, and we develop novel algorithms that enable us to accomplish this cheaply and quickly for standard LLM APIs.

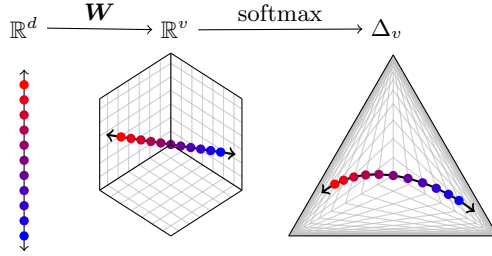


Figure 1: LLM outputs are constrained to a low-dimensional subspace of the full output space. We can use this fact to glean information about API-protected LLMs by analyzing their outputs. Here we show how a toy LLM’s low-dimensional embeddings in \mathbb{R}^d (illustrated here as a 1-D space) are transformed linearly into logits in \mathbb{R}^v (here, a 3D space) via the softmax matrix \mathbf{W} . The resulting outputs lie within a $(d = 1)$ -dimensional subspace of the output space. The softmax function also preserves this low-dimensionality when transforming the logits into probabilities distributions on Δ_v . We call this low-dimensional subspace the *image* of the model. We can obtain a basis for the image of an API-protected LLM by collecting d of its outputs. The LLM’s image can reveal non-public information, such as the LLM’s embedding size, but it can also be used for accountability, such as verifying which LLM an API is serving.

Table 1: An overview of our proposed applications that exploit LLM images.

Application	Section
Efficiently extract full LLM outputs.	3
Find the embedding size of an LLM and guess its parameter count.	4
Identify which LLM produced a given output.	5
Detect when and what type of LLM updates occur.	5.1
Find tokenization bugs (unargmaxable tokens).	6.1
Approximately reconstruct the LLM’s softmax matrix.	6.2
Cheaply and accurately reconstruct “hidden prompts”.	6.3
Implement basis-aware decoding algorithms.	6.4

Obtaining the LLM image (§2) allows to explore several capabilities that cover a broad set applications, and empirically verify several of them. For instance, we design and empirically verify an algorithm for finding the embedding size of an API-based LLM, and demonstrate the effectiveness of our method by estimating the embedding size of `gpt-3.5-turbo`, a closed-source API-protected LLM, to be 4,096. We also empirically show effectiveness of using LLM images as unique *signatures* that can be used to identify outputs from a model with high accuracy, a useful property for API LLM accountability. The sensitivity of these signatures to slight changes in the LLM parameters also makes them suitable for inferring granular information about model parameter updates.

Considering several proposals to mitigate this vulnerability, we find no obvious fix to prevent obtaining LLM images without dramatically altering the LLM architecture. While providers may choose to alter the API to hide this information, the relevant API features have valuable and safe use cases for the LLM clients, who may rely on access to features like logit bias. Though our findings be viewed as a warning to LLM providers to carefully consider the consequences of their LLM architectures and APIs, we prefer to view our findings as a potential *feature* that LLM providers may choose to keep in order to better maintain trust with their customers by allowing outside observers to audit their model.

2 LLM outputs are restricted to a low-dimensional linear space

Consider the architecture of a typical LLM, depicted in Figure 2. A Transformer with embedding size d outputs a low-dimensional *contextualized embedding* $\mathbf{h} \in \mathbb{R}^d$ (or simply *embedding*). Projecting the embedding onto \mathbb{R}^v via the linear map defined by the LLM’s *softmax matrix* \mathbf{W} , we obtain the *logits* $\ell = \mathbf{W}\mathbf{h}$. Because \mathbf{W} is in $\mathbb{R}^{v \times d}$, its rank (i.e., number of linearly independent columns) is at most d . The rank of a matrix corresponds to the dimension of the *image* of the linear map it defines, i.e., the vector space comprising the set of possible outputs of the function. In other words, if the linear map w is defined as $w(\mathbf{h}) = \mathbf{W}\mathbf{h}$, then w ’s image $\text{im}(w) = \{w(\mathbf{h}) \in \mathbb{R}^v : \mathbf{h} \in \mathbb{R}^d\}$

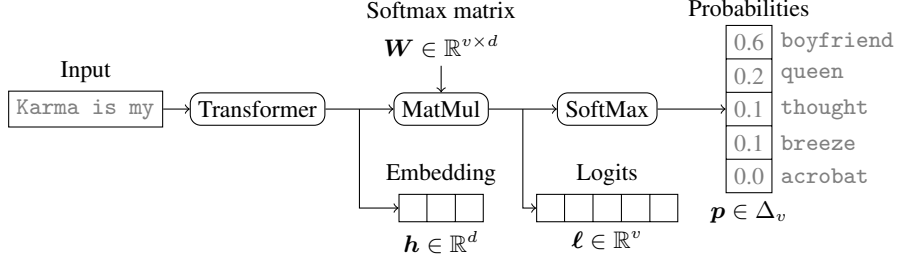


Figure 2: A typical language model architecture. After the input is processed by a neural network, usually a transformer [Vaswani et al., 2017], into a low-dimensional embedding \mathbf{h} , it is multiplied by the softmax matrix \mathbf{W} , projecting it linearly from \mathbb{R}^d onto \mathbb{R}^v to obtain the logit vector ℓ . The softmax function is then applied to the logit vector to obtain a valid probability distribution \mathbf{p} over next-token candidates.

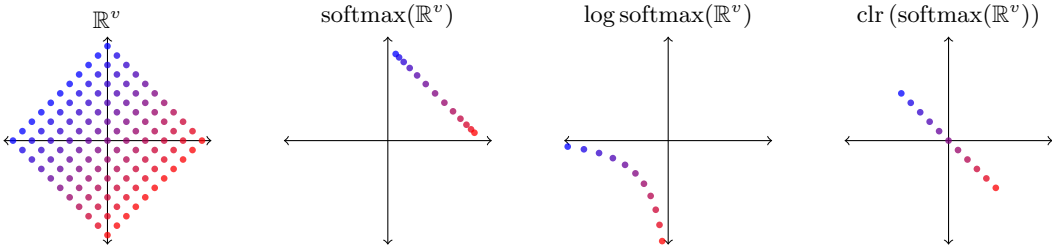


Figure 3: Points in the logit space \mathbb{R}^v (far left) are mapped via the softmax function to points (probability distributions) on the simplex Δ_v (middle left). Crucially, the softmax maps all points that lie on the same diagonal (shown as points of the same color) to the same probability distribution. For numerical stability, these values are often stored as log-probabilities (middle right). The clr transform returns probability distributions to points to a subspace U_v of the logit space (far right). The softmax function and clr transform are inverses of one another, and form an isomorphism between U_v and Δ_v .

is a d -dimensional subspace of \mathbb{R}^v . Thus, the LLM’s logits will always lie on the d -dimensional¹ subspace of \mathbb{R}^v .

We now turn our attention to the LLM’s final output: the next-token distribution \mathbf{p} . Due to the softmax function, this is a valid probability distribution over v items, meaning it is a v -tuple of real numbers between 0 and 1 whose sum is 1. The set of valid probability distributions over v items is referred to as the v -simplex, or Δ_v . Perhaps surprisingly, Δ_v is also a valid vector space (albeit under a non-standard definition of addition and scalar multiplication) and is isomorphic to a $(v - 1)$ -dimensional vector subspace of \mathbb{R}^v [Aitchison, 1982, Leinster, 2016]. In particular, it is isomorphic to the hyperplane U_v that is perpendicular to the all-ones vector $\mathbf{1}_v$, as illustrated in Figure 3. The softmax function is thus an isomorphism $U_v \rightarrow \Delta_v$ whose inverse mapping $\Delta_v \rightarrow U_v$ is the center log ratio transform (clr), which is defined as

$$\text{clr}(\mathbf{p}) = \log \frac{\mathbf{p}}{(\prod_{i=1}^v p_i)^{\frac{1}{v}}} = \log \mathbf{p} - \frac{1}{v} \sum_{i=1}^v \log p_i. \quad (1)$$

Observe also that the function $\ell \mapsto \text{clr}(\text{softmax}(\ell))$ projects ℓ linearly onto the nearest point in U_v . By this linearity, and the fact that $\text{im}(w)$ is a d -dimensional subspace of \mathbb{R}^v , we can observe that $\text{im}(\text{softmax} \circ w)$ and $\text{im}(\text{clr} \circ \text{softmax} \circ w)$ are also d -dimensional vector subspaces of Δ_v and $U_v \subset \mathbb{R}^v$ respectively. Interpreted, this means that the LLM’s outputs occupy d -dimensional subspaces of the logit space \mathbb{R}^v , probability space Δ_v , and U_v . We call these subspaces the *image* of the LLM on each given space. A natural consequence of the low-dimensional output space is that any collection of d linearly independent LLM outputs $\mathbf{p}^1, \mathbf{p}^2, \dots, \mathbf{p}^d$ form a basis for the image of the model, i.e., all LLM outputs can be expressed as a unique linear combination of these d outputs [Yang et al., 2018, Finlayson et al., 2023].

¹More accurately, the logits will always lie on an *at-most- d* -dimensional subspace. For convenience, we assume full-rank matrices, and thus a d -dimensional subspace.

Table 2: A summary of our proposed algorithms, with estimates for the number of API calls required per output, and the price of acquiring the model image. Estimates are based on a gpt-3.5-turbo-like API LLM with $v = 100\text{K}$, $d = 4096$, $\epsilon = 10^{-6}$, $k = 5$, $b_{\max} = 100$, and $n = 4$. Note that the $O(d)$ algorithm cannot be used to obtain the LLM image, since it relies on having LLM image as a preprocessing step.

Algorithm	Complexity	API calls per output	Image price
Logprob-free	$O(v \log \frac{1}{\epsilon})$	800K	\$16,384
With logprobs	v/k	20K	\$410
Numerically stable	$v/(k-1)$	25K	\$512
Stochastically robust	$nv/(k-2)$	133K	\$2,724
LLM Image	$O(d)$	1K–32K	-

The rest of this paper discusses the implications and applications of this mathematical fact for API-protected LLMs, starting with methods for finding the LLM image given a restrictive API, then using the LLM image for various purposes.

3 Fast, full outputs from API-protected LLMs

There are several uses for full-vocab LLM outputs, however most LLM APIs do not return full outputs. This is likely because full outputs are large and expensive to send over an API, but could also be to prevent abuse of APIs, such as using these outputs to distill models [Hinton et al., 2015, Mukherjee and Awadallah, 2019, Hsieh et al., 2023] or discover proprietary information (see Section 4). In their paper, Morris et al. [2023] give an algorithm for recovering these full outputs from restricted APIs by taking advantage of a common API option that allows users to add bias to the logits for specific tokens. The algorithm they describe requires $O(v \log \frac{1}{\epsilon})$ calls to the API to obtain one full output with precision ϵ .

We give an improvement that theoretically obtains full outputs in v/k API calls for APIs that return the log-probability of the top- k tokens. We find that this improved algorithm suffers from numerical instability, and give a numerically stable algorithm that obtains full outputs in $v/(k-1)$ API calls.

Next, we give a practical algorithm for dealing with stochastic APIs that randomly choose outputs from a set of n possible outputs. This algorithm allows the collection of full outputs in less than $nv/(k-2)$ API calls on average.

Finally, we reduce the number of API calls in all of the above algorithms from $O(v)$ to $O(d)$ by adding in a preprocessing step to find the low-dimensional image of the LLM. This speedup makes obtaining full LLM outputs up to 100 times faster and cheaper, depending on the LLM. Table 2 gives an overview of our algorithms with back-of-the-envelope cost estimates for a specific LLM.

3.1 Fast, full outputs from APIs with logprobs

Our goal is to recover a full-vocabulary next-token distribution $\mathbf{p} \in \Delta_v$ from an API-protected LLM. We will assume that the API accepts a prompt on which to condition the distribution, as well as a list of up to k tokens and a bias term $b \leq b_{\max}$ to add to the logits of the listed tokens before applying the softmax function. The API returns a record with the k most likely tokens and their probabilities from the biased distribution. For instance, querying the API with k maximally biased tokens, which without loss of generality we will identify as tokens $1, 2, \dots, k$, yields the top- k most probable tokens from the *biased* distribution $\mathbf{p}' = \text{softmax}(\ell')$ where

$$\ell'_i = \begin{cases} \ell_i + b_{\max} & i \in \{1, 2, \dots, k\} \\ \ell_i & \text{otherwise} \end{cases}$$

and $\ell \in \mathbb{R}^v$ is the LLM’s logit output for the given prompt.

Assuming that the logit difference between any two tokens is never greater than b_{\max} , these top- k biased probabilities will be p'_1, p'_2, \dots, p'_k . For each of these biased probabilities p'_i , we can solve for

the unbiased probability as

$$p_i = \frac{p'_i}{\exp b_{\max} - \exp b_{\max} \sum_{j=1}^k p'_j + \sum_{j=1}^k p'_j} \quad (2)$$

(proof in the Appendix A.1). Thus, for each API call, we can obtain the unbiased probability of k tokens, and obtain the full distribution in v/k API calls.

3.2 Numerically stable full outputs from APIs

In practice, the algorithm described in Section 3.1 suffers from severe numerical instability, which can be attributed to the fast-growing exponential term $\exp b_{\max}$, and the term $\sum_{j=1}^k p'_j$ which quickly approaches 1. We can eliminate the instability by sacrificing some speed and using a different strategy to solve for the unbiased probabilities. Without loss of generality, let p_v be the maximum unbiased token probability. This can be obtained by querying the API once with no bias. If we then query the API and apply maximum bias to only tokens $1, 2, \dots, 1 - k$, then the API will yield $p'_1, p'_2, \dots, p'_{k-1}$ and p'_v . We can then solve for the unbiased probabilities of the $k - 1$ tokens

$$p_i = \exp(\log p'_i - b_{\max} - \log p'_v + \log p_v) \quad (3)$$

(proof in Appendix A.2). By finding $k - 1$ unbiased token probabilities with every API call, we obtain the full output in $v/(k - 1)$ calls total.

3.3 Full outputs from stochastic APIs

Each of the above algorithms assume that the API is deterministic, i.e., the same query will always return the same output. This is not always the case. For instance, we find that OpenAI’s LLM APIs are *stochastic*. While this would seem to doom any attempt at obtaining full outputs from the LLM, we find that certain types of stochasticity can be dealt with. In particular, we model OpenAI’s stochastic behavior as a collection of n outputs $\mathbf{p}^{(1)}, \mathbf{p}^{(2)}, \dots, \mathbf{p}^{(n)}$ from which the API randomly returns from. This might be the result of multiple instances of the LLM being run on different hardware which results in slightly different outputs. Whichever instance the API returns from determines which of the n outputs we get. In order to determine which of the outputs the API returned from, assume without loss of generality that $p_{v-1}^{(i)}$ is the second highest token probability for all i , and observe that

$$\log p_v^{(i)} - \log p_{v-1}^{(i)} = \log p'_v{}^{(i)} - \log p'_{v-1}{}^{(i)} \quad (4)$$

for all outputs $\mathbf{p}^{(i)}$ and unbiased outputs $\mathbf{p}'^{(i)}$ where tokens v and $v - 1$ are not biased (proof in Appendix A.3). Therefore, by biasing only $k - 2$ tokens for each call, the API will return $p_1^{(i)}, p_2^{(i)}, \dots, p_{k-2}^{(i)}$ as well as $p'_v{}^{(i)}$ and $p'_{v-1}{}^{(i)}$ for some i , and we can determine which output $\mathbf{p}^{(i)}$ the result comes from by using $\log p'_v{}^{(i)} - \log p'_{v-1}{}^{(i)}$ as an identifier. Thus, after an average of $nv/(k - 2)$ calls to the API we can collect the full set of probabilities for one of the outputs.

3.4 Ultra-fast full outputs using the LLM image

So far, the dominating factor in each algorithm’s runtime is v . We now introduce a preprocessing step that takes advantage of the low-dimensional LLM output space to obtain $O(d)$ versions of all the above algorithms. Since $d \ll v$ for many modern language models, this modification can result in multiple orders of magnitude speedups, depending on the LLM. For instance, the speedup for an LLM like *pythia-70m* would be $100\times$. The key to this algorithm is the observation from Section 2 that d linearly independent outputs from the API constitute a basis for the whole output space (since the LLM’s image has dimension d). We can therefore collect these outputs

$$\mathbf{P} = [\mathbf{p}^1 \quad \mathbf{p}^2 \quad \dots \quad \mathbf{p}^d] \in \Delta_v^d$$

as a preprocessing step in $O(vd)$ API calls using any of the above algorithms and d unique prompts, and then use these to reconstruct the full LLM output after only $O(d)$ queries for each subsequent output.

To get a new full output \mathbf{p} , use any of the above algorithms to obtain p_1, p_2, \dots, p_d . Next, we will use the additive log ratio (alr) transform, which an isomorphism $\Delta_v \rightarrow \mathbb{R}^{v-1}$ and is defined as

$$\text{alr}(\mathbf{p}) = \left(\log \frac{p_2}{p_1}, \log \frac{p_3}{p_1}, \dots, \log \frac{p_v}{p_1} \right)$$

to transform the columns of \mathbf{P} and \mathbf{p} into vectors in \mathbb{R}^{v-1} , though since we only know the first d values of \mathbf{p} , we can only obtain the first d values of $\text{alr}(\mathbf{p})$. Because the alr transform is an isomorphism, we have that the columns of

$$\text{alr}(\mathbf{P}) = [\text{alr}(\mathbf{p}^1) \quad \text{alr}(\mathbf{p}^2) \quad \dots \quad \text{alr}(\mathbf{p}^d)] \in \mathbb{R}^{(v-1) \times d}$$

form a basis for a d -dimensional vector subspace of \mathbb{R}^{v-1} , and $\text{alr}(\mathbf{p})$ lies within this subspace. Therefore, there is some $\mathbf{x} \in \mathbb{R}^d$ such that $\text{alr}(\mathbf{P})\mathbf{x} = \text{alr}(\mathbf{p})$. To solve for \mathbf{x} , all that is required is to find the unique solution to the first d rows of this system of linear equations

$$\begin{bmatrix} \text{alr}(p^1)_1 & \text{alr}(p^2)_1 & \dots & \text{alr}(p^d)_1 \\ \text{alr}(p^1)_2 & \text{alr}(p^2)_2 & \dots & \text{alr}(p^d)_2 \\ \vdots & \vdots & \ddots & \vdots \\ \text{alr}(p^1)_d & \text{alr}(p^2)_d & \dots & \text{alr}(p^d)_d \end{bmatrix} \begin{bmatrix} x_1 \\ x_2 \\ \vdots \\ x_d \end{bmatrix} = \begin{bmatrix} \text{alr}(p)_1 \\ \text{alr}(p)_2 \\ \vdots \\ \text{alr}(p)_d \end{bmatrix}. \quad (5)$$

After finding \mathbf{x} , we can reconstruct the full LLM output $\mathbf{p} = \text{alr}^{-1}(\text{alr}(\mathbf{P})\mathbf{x})$, where the inverse alr function is defined as

$$\text{alr}^{-1}(\mathbf{x}) = \frac{1}{1 + \sum_{i=1}^{v-1} \exp x_i} \cdot (1, \exp x_1, \exp x_2, \dots, \exp x_{v-1}).$$

Thus we can retrieve \mathbf{p} in only $O(d)$ API queries.

This $(v/d) \times$ speedup makes any method that relies on full model outputs significantly cheaper. This includes model stealing [Tramèr et al., 2016] which attempts to learn a model that exactly replicates the behavior of a target model.

4 Discovering the embedding size of API-protected LLMs

Without knowing the exact architectural details, other than assuming the generic output layer described in Figure 2, it is possible to infer the embedding size d of an API-protected language model from its outputs alone. This is a direct result of the fact that the model outputs occupy a d -dimensional subspace of Δ_v , and therefore collecting d linearly independent outputs $\mathbf{p}_1, \mathbf{p}_2, \dots, \mathbf{p}_d \in \Delta_v$ from the LLM will form a basis for the LLM’s image, meaning that all subsequent model outputs \mathbf{p}_{d+1} will be a linear combination of the first d outputs. Assuming that model outputs are full rank, i.e., all collections of d prompts are linearly independent, and all collections of $d + 1$ prompts are linearly dependent, we can discover the value of d by collecting outputs one at a time until the number of linearly independent outputs in the collection stops increasing, which will occur when we have collected $d + 1$ prompts. In practice, we find that this full-rank assumption tends to hold well enough when over-collecting outputs, e.g., collecting $d + 1000$ outputs.

To find the dimension of a space spanned by model outputs, we use the fact that a matrix with d linearly independent columns will have d non-zero singular values. We can therefore plot the singular values of the matrix

$$\mathbf{L} = \text{clr}(\mathbf{P}) = [\text{clr}(\mathbf{p}_1) \quad \text{clr}(\mathbf{p}_2) \quad \dots \quad \text{clr}(\mathbf{p}_n)]$$

and observe the index at which the magnitude of the singular values drops to zero, which will occur at index d .² In practice, due to precision issues, the magnitudes may not drop all the way to zero.

To validate our method, we collect next-token distributions (conditioned on unique, 1-token prompts) from several open-source LLMs from the Pythia family [Biderman et al., 2023] with embedding sizes ranging from 512 to 1024. For all these models, we find that the singular values of the resulting

²We will loosely refer to \mathbf{L} as the logit matrix, though these are technically the logits projected onto the nearest point on U_v .

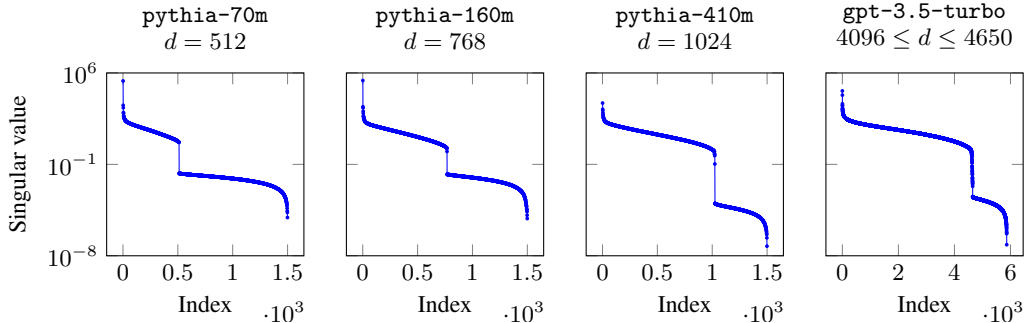


Figure 4: The singular values of outputs from LLMs with various known and unknown embedding sizes d . For each model with known embedding size, there is a clear drop in magnitude at singular value index d , indicating the embedding size of the model. Using this observation, we can guess the embedding size of gpt-3.5-turbo.

output matrix drop dramatically precisely at the index corresponding to the embedding size of the model, as shown in the first three plots of Figure 2.

To demonstrate our method’s effectiveness against API-protected LLMs, we use our stochastically robust $nv/(k-2)$ algorithm to collect nearly 6,000 next-token distribution outputs from gpt-3.5-turbo³, a popular API-protected LLM whose embedding size is not publicly disclosed. We find that the singular values for these outputs drop dramatically between index 4,600 and 4,650, indicating that the embedding size of this model is at most this size. This predicted embedding size is somewhat abnormal, since LLM embedding sizes are traditionally set to powers of two (or sums of powers of two). If this were the case for gpt-3.5-turbo, it would be reasonable to guess that the embedding size is $2^{12} = 4096$ or $2^{12} + 2^9 = 4608$, the former of which we think is most likely. We predict that our raw estimate of 4,600-4,650 is an overestimate of the true embedding size, since any abnormal outputs due to errors (whether in our own code or OpenAI’s) would only increase the dimensionality of the observed output space. In particular, if we inadvertently collected 504 corrupted outputs, then a model with embedding size 4,096 would appear to have an embedding size of 4,600.

Extrapolating further, assuming that gpt-3.5-turbo has a similar architecture to most transformer-based LLMs, it is likely that the number of parameters in gpt-3.5-turbo is around 7 billion. This estimation is based on the fact that most known transformer-based LLMs with embedding size 4,096 have ≈ 7 billion parameters. Any other parameter count would result in either abnormally narrow or wide neural networks which are not known to have favorable performance. An important exception to this rule-of-thumb, however, would be the increasingly popular “mixture-of-experts” architecture which tends to have many more parameters per embedding dimension.

Previous estimates of gpt-3.5-turbo’s parameter count based on hearsay have generally exceeded 7B [Singh et al., 2023], however given the periodically updating versions and decreasing cost of inference with this model, it is possible that its size and architecture has changed over time. Fortunately, our method can be used to monitor these updates over time, alerting end-users when LLM providers make architectural changes to their model, specifically updates to the embedding size and/or parameter count.

5 Identifying LLMs from a single output

The image of two different LLMs, even different checkpoints from the same LLM, are largely disjoint. As shown in Figure 5, the logit output from a late-training checkpoint of Pythia-70M lies uniquely in the image of the checkpoint, and not in the image of the preceding or following checkpoints. We also verify that the output does not lie in the image of any checkpoints from a similar LLM trained on deduplicated data, nor any checkpoint from a larger LLM trained on the same data. This suggests that the image of a LLM is highly sensitive to small parameter changes. Intuitively this makes sense, since the output of one model will only be in the image of another model in the extremely unlikely event that

³We specifically use model version 0125, accessed February 1–19, 2024.

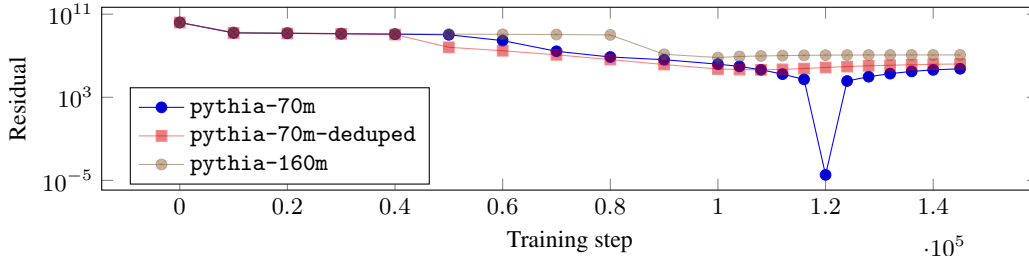


Figure 5: Residuals of the least-squares solution of $\mathbf{W}\mathbf{x} = \ell$ for an output ℓ from a pythia-70m checkpoint (training step 120K), and softmax matrices \mathbf{W} at various training steps for pythia-70m, and pythia-70m-deduped, and pythia-160m. Low/high residual values indicate that the output ℓ is/is not in a model’s image. Residuals for pythia-70m decrease as the checkpoints near the checkpoint that generated the output, but remain high. Note that this test works even if the softmax matrices \mathbf{W} are substituted with model outputs \mathbf{L} .

Table 3: Implications of image/logit changes.

Change	Interpretation
No logit change, no image change	No update
Logit change, no image change	Hidden prompt change or partial finetune with frozen output layer
Low-rank image change (See § 5.2)	LoRA update
Image change	Full finetune

it happens to lie on the low-dimensional ($< d$) intersection of the models’ images. Mathematically the dimension of the models’ images’ intersection is small since the intersection $U \cap V$ of two subspaces U and V that are not subsets of one another has dimension $\dim U + \dim V - \dim(U \cup V)$, which implies that $\dim(U \cap V) < \min\{\dim U, \dim V\}$ (since $\dim(U \cup V) > \max\{\dim U, \dim V\}$). Thus, it is possible to determine precisely which LLM produced a particular output, using only API access to a set of LLMs and without knowing the exact inputs to the model. In this way, the model’s image acts as a *signature* for the model, i.e., a unique model identifier.

This finding has implications for LLM provider accountability. For instance, if provider A suspects provider B of stealing their proprietary model, provider A could check provider B ’s model signature to see if it matches their own. It would be extremely unlikely that the signatures match if the LLMs are not the same. Similarly, if a provider claimed to be serving a proprietary model while in actuality attempting to profit off of an open-source model with a non-commercial license, an auditor again could discover this by checking the LLM signature. This test is somewhat one-sided, however, since a clever provider may do a small amount of additional fine-tuning to change their stolen LLM’s image.

5.1 Detecting and disambiguating LLM updates

Another practical application of highly sensitive LLM images is to detect and distinguish minor and major model updates to API-protected LLMs. Using the above test, we can tell whether or not the LLM image remains the same, even if the logit outputs change. This phenomenon would correspond to a partial model update, where some part of the model changes, but the softmax matrix remains the same. An example of this would be if the LLM has a hidden prefix added to all prompts and this hidden prefix changes: the model’s outputs will change but the image will remain the same. Table 3 gives an overview for how to interpret various combinations of detectable API changes, This information is useful for monitoring unannounced changes in API LLMs.

5.2 Detecting LoRA updates

We speculate that it is possible to gain even higher granularity information on LLM updates of certain types, such as LoRA [Hu et al., 2022] updates. LoRA is a popular parameter-efficient fine-tuning method which adjusts model weights with a low-rank update \mathbf{AB} where $\mathbf{A} \in \mathbb{R}^{v \times r}$ and $\mathbf{B} \in \mathbb{R}^{r \times d}$ so that the softmax matrix $\mathbf{W} \in \mathbb{R}^{v \times d}$ becomes $\mathbf{W} + \mathbf{AB}$. We speculate that it is possible to detect

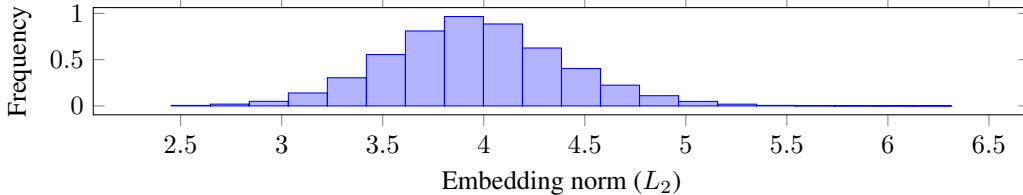


Figure 6: Softmax matrix row magnitudes (here from pythia-70m) are small and are distributed approximately normally within a narrow range.

these types of updates by collecting LLM outputs before ($\mathbf{L} \in \mathbb{R}^{v \times d}$) and after ($\mathbf{L}' \in \mathbb{R}^{v \times d}$) the update and decomposing them as $\mathbf{W}\mathbf{H} = \mathbf{L}$ and $(\mathbf{W} + \mathbf{A}\mathbf{B})\mathbf{H} = \mathbf{L}'$ where $\mathbf{H}, \mathbf{H}' \in \mathbb{R}^{d \times d}$ such that $\text{im}(\mathbf{W}\mathbf{H}) = \text{im}(\mathbf{W} + \mathbf{A}\mathbf{B})$. If such a decomposition is found, then it appears likely that the weights received a low-rank update of rank r . We leave it to future work to determine whether finding such a decomposition is sufficient to conclude that a LoRA update took place, as well as to find an efficient algorithm for finding such a decomposition.

6 More applications

Access to the LLM’s image can lead to many other capabilities, some of which we discuss below. We leave further investigation of these methods for future work.

6.1 Finding unargmaxable tokens

Due to the low-rank constraints on LLM outputs, it is possible that some tokens become *unargmaxable* [Demeter et al., 2020, Grivas et al., 2022], i.e., there is a token i such that the constraints disallow any output \mathbf{p} with $\arg \max_i p_i = i$. This happens when the LLM’s embedding representation of i lies within the convex hull of the other tokens’ embeddings. Previously, finding unargmaxable tokens appeared to require full access to the softmax matrix \mathbf{W} . Interestingly, we find that it is possible to identify unargmaxable tokens using only the LLM’s image, which our method is able to recover. This technique allows API customers to find quirks in LLM behavior such as tokens that the model is unable to output (at least under greedy decoding).

6.2 Recovering the softmax matrix from outputs

Since our method gives us access to the image of the output layer, and not the output layer parameters, we investigate the how one might reconstruct the output layer parameters, either exactly or approximately. We hypothesize that LLM embeddings generally lie near the surface of a hypersphere in \mathbb{R}^d with a small radius r . We see evidence of this in the fact that the Pythia LLM embedding norms are all small and roughly normally distributed, as shown in Figure 6.

Assuming this holds for any LLM, we can attempt to recover \mathbf{W} up to a rotation by simplifying the assumption into a constraint that all embeddings must have a magnitude of 1. Then, given a matrix $\mathbf{L} \in \mathbb{R}^{n \times v}$ of model logits, we can find \mathbf{W} (up to a rotation) by finding a decomposition $\mathbf{W}\mathbf{H} = \mathbf{L}$ such that for all i , $\|\mathbf{W}_i\|_2 = r$. This solution may also be approximated by finding the singular value decomposition $\mathbf{W}\mathbf{\Sigma}\mathbf{V}^T$ of \mathbf{L} , though it is likely that all rows of this \mathbf{W} will have magnitude less than 1 and they are not guaranteed to be normally distributed.

6.3 Improved LLM inversion

Morris et al.’s [2023] recent approach to recovering hidden prompts (i.e., an additional prefix added to LLM input, not shown to the user) uses full LLM API outputs to train an “inversion” model that generates the prefix conditioned on the LLM’s full logprob vector $\log \mathbf{p}$. In addition to our algorithm from Section 3.4 making this much cheaper to implement, we also propose a methodological change to their procedure. In particular, to deal with the size mismatch between the LLM’s vocabulary size v and the inversion model’s embedding size d_{inv} , Morris et al. [2023] pad and reshape the vector into a

$\lceil v/d_{\text{inv}} \rceil$ -length sequence of embeddings in $\mathbb{R}^{d_{\text{inv}}}$. This transformation is somewhat unnatural, and requires that the inversion model only be conditioned on a single output.

We propose instead to take advantage of our knowledge of the LLM’s image to obtain a linearly lossless representation of the LLM output in \mathbb{R}^d , which is much closer to the inversion model size, then use an MLP to project this representation onto $\mathbb{R}^{d_{\text{inv}}}$ to feed into the inversion model. Formally, after obtaining \mathbf{P} and \mathbf{p} from the API, we use the unique solution \mathbf{x} to $\text{clr}(\mathbf{P})\mathbf{x} = \text{clr}(\mathbf{p})$ as the input to the inversion model. This modification has an additional advantage: instead of conditioning on a single output \mathbf{p} , the LLM can be used to generate a short sequence of outputs $\mathbf{p}^1, \mathbf{p}^2, \dots, \mathbf{p}^n$ which can be fed into the inversion model as $\mathbf{x}^1, \mathbf{x}^2, \dots, \mathbf{x}^n$ where $\text{clr}(\mathbf{P})\mathbf{x}^i = \text{clr}(\mathbf{p}^i)$. We leave the implementation and evaluation of this proposed modification for future work. This technique can be applied generally to any method that takes LLM outputs as input.

6.4 Basis-aware sampling

In a recent paper, Finlayson et al. [2023] propose a decoding algorithm that avoids type-I sampling errors by identifying tokens that must have non-zero true probability. Importantly, this method relies on knowing the basis of the LLM’s output space, and is therefore only available for LLMs whose image is known. Our proposed approach for finding the image of API-protected LLMs makes this decoding algorithm possible for API LLMs.

7 Mitigations

We consider a three proposals that LLM providers may take to guard against our methods. The first proposal is to remove API access to logprobs. This, however is theoretically insufficient, as Morris et al. [2023] show that it is possible to obtain full outputs using only information about the biased argmax token, albeit inefficiently in $v \log \epsilon$ API calls. Regardless of the theoretical result, providers may rely on the extreme inefficiency of the algorithm to protect the LLM. This appears to be the approach OpenAI took after learning about this vulnerability from Carlini et al. [2024], by always returning the top- k *unbiased* logprobs. Our new proposed algorithm, however, brings the number of queries down to a more feasible $d \log \epsilon$ API calls once the initial work of finding the LLM image has finished, weakening the argument that the expensiveness of the algorithm is sufficient to disregard our technique.

The next proposal is to remove API access to logit bias. This would be an effective way to protect the LLM, since there are no known methods to recover full outputs from such an API. However, the logit bias interface is presumably useful for many clients who might be disappointed by its shutdown.

Lastly, we consider alternative LLM architectures that do not suffer from a softmax bottleneck. There are several such proposed architectures with good performance. Though this is the most expensive of the proposed defenses, due to the requirement of training a new LLM, it would have the beneficial side effect of also treating other tokenization issues that plague large-vocabulary LLMs [e.g., Itzhak and Levy, 2022]. A transition to softmax-bottleneck-free LLMs would fully prevent our attack, since the model’s image would be the full output space.

8 Discussion

Overall, the potential applications of our methods can have great impact in building trust between the LLM API users and the providers; at the same time, none are particularly harmful to LLM providers. For instance, consider discovering the embedding size of the LLM, which is often non-public information in proprietary LLMs. However, access to this hyperparameter does not enable a competitor to fully recover the parameters of the LLM’s softmax matrix or boost performance of their own model; several other factors such as training data mix, human feedback and several other engineering choices are still critical and hidden. Even using model outputs to steal hidden prompts (see Section 6.3) is unlikely to have detrimental effects, as hidden prompt leakage is a known vulnerability and best practice dictates that no private information should be contained in these system prompts [Greshake et al., 2023, Liu et al., 2023]. We find that the most dangerous consequence of our findings might simply be that model stealing methods that rely on full outputs get cheaper by a factor of v/d , which in the case of gpt-3.5-turbo amounts to about $25\times$.

On the other hand, allowing LLM API users to detect model changes builds trust between LLM providers and their customers, and leads to greater accountability and transparency for the providers. Our method can be used to implement efficient protocols for model auditing without exposing the model parameters or detailed configuration information, which may help model safety and privacy protection of personalized, proprietary models. We therefore take the position that our proposed methods and findings do not necessitate a change in LLM API best practices, but rather expand the tools available to API customers, while warning LLM providers of the information their APIs expose.

9 Simultaneous discovery

In a remarkable case of simultaneous discovery, Carlini et al. [2024] propose a very similar approach to ours for gaining insight into API-protected LLMs. Here we review a some interesting interactions between our work and theirs. First, we give an algorithm for obtaining full outputs in v/k API calls, while their algorithm corresponds to our $v/(k-1)$ algorithm. This has little impact on our final result, since our v/k algorithm suffers from numerical instability, but it is an interesting theoretical result nonetheless. On the flip side, Carlini et al. propose an improved logprob-free method for getting full outputs from an API that takes advantage of parallel queries. This useful method is actually complementary to our $O(d)$ algorithm, since they can be combined to yield an even better algorithm for obtaining full outputs.

Next, our experiments with OpenAI’s API were fraught with issues of stochasticity: the API would return different results for the same query, leading us to develop the stochastically robust full output algorithm. Meanwhile, our colleagues did not appear to encounter such issues, perhaps because they had access to a more stable API endpoint than ours.

Lastly, Carlini et al. focus mostly on defenses and mitigations against attacks, while our own work focuses more on understanding the capabilities such attacks provide once an LLM image has been obtained. These approaches complement each other, since our work provides additional motivation for why (or why not) such defenses should be implemented.

10 Conclusion

In this paper we have laid out the fundamentals of how the softmax bottleneck imposes the low-rank constraints on LLM outputs, and shown how these constraints expose non-public information about API-protected LLMs. We have explained how this information, i.e., the LLM’s image, lends itself to a *model signature*, which has myriad uses—exposing model hyperparameters, recovering the output layer parameters, detecting specific types of model updates, and efficiently obtaining full outputs from the model, among others. We find that current protections against these attacks may be insufficient, and that the more effective guards we consider either eliminate sanctioned API use cases (i.e., logit bias), or are expensive to implement (i.e., changing model architecture). Lastly, we argue that this “vulnerability” may be more of a feature than a bug; since we believe that the benefits for API clients outweigh any known harms to LLM providers.

11 Acknowledgements

We thank Jack Morris and Vitaly Shmatikov for their insights and feedback on this work.

References

- J. Aitchison. The statistical analysis of compositional data. *Journal of the Royal Statistical Society: Series B (Methodological)*, 44(2):139–160, 1982. doi: <https://doi.org/10.1111/j.2517-6161.1982.tb01195.x>. URL <https://rss.onlinelibrary.wiley.com/doi/abs/10.1111/j.2517-6161.1982.tb01195.x>. 2
- Stella Biderman, Hailey Schoelkopf, Quentin Gregory Anthony, Herbie Bradley, Kyle O’Brien, Eric Hallahan, Mohammad Aflah Khan, Shivanshu Purohit, USVSN Sai Prashanth, Edward Raff, et al. Pythia: A suite for analyzing large language models across training and scaling. In *International Conference on Machine Learning*, pages 2397–2430. PMLR, 2023. 4

- Nicholas Carlini, Daniel Paleka, Krishnamurthy Dj Dvijotham, Thomas Steinke, Jonathan Hayase, A. Feder Cooper, Katherine Lee, Matthew Jagielski, Milad Nasr, Arthur Conmy, Eric Wallace, David Rolnick, and Florian Tramèr. Stealing part of a production language model, 2024. 7, 9
- David Demeter, Gregory Kimmel, and Doug Downey. Stolen probability: A structural weakness of neural language models. In Dan Jurafsky, Joyce Chai, Natalie Schluter, and Joel Tetreault, editors, *Proceedings of the 58th Annual Meeting of the Association for Computational Linguistics*, pages 2191–2197, Online, July 2020. Association for Computational Linguistics. doi: 10.18653/v1/2020.acl-main.198. URL <https://aclanthology.org/2020.acl-main.198>. 6.1
- Matthew Finlayson, John Hewitt, Alexander Koller, Swabha Swayamdipta, and Ashish Sabharwal. Closing the curious case of neural text degeneration. *ArXiv*, abs/2310.01693, 2023. URL <https://api.semanticscholar.org/CorpusID:263608672>. 2, 6.4
- Kai Greshake, Sahar Abdelnabi, Shailesh Mishra, Christoph Endres, Thorsten Holz, and Mario Fritz. Not what you’ve signed up for: Compromising real-world llm-integrated applications with indirect prompt injection. *Proceedings of the 16th ACM Workshop on Artificial Intelligence and Security*, 2023. URL <https://api.semanticscholar.org/CorpusID:258546941>. 8
- Andreas Grivas, Nikolay Bogoychev, and Adam Lopez. Low-rank softmax can have unargmaxable classes in theory but rarely in practice. In *Proceedings of the 60th Annual Meeting of the Association for Computational Linguistics (Volume 1: Long Papers)*, pages 6738–6758, Dublin, Ireland, May 2022. Association for Computational Linguistics. doi: 10.18653/v1/2022.acl-long.465. URL <https://aclanthology.org/2022.acl-long.465>. 6.1
- Geoffrey Hinton, Oriol Vinyals, and Jeff Dean. Distilling the knowledge in a neural network. In *Proc. of NeurIPS*, 2015. URL <https://arXiv.org/abs/1503.02531>. 3
- Cheng-Yu Hsieh, Chun-Liang Li, Chih-Kuan Yeh, Hootan Nakhost, Yasuhisa Fujii, Alexander J. Ratner, Ranjay Krishna, Chen-Yu Lee, and Tomas Pfister. Distilling step-by-step! outperforming larger language models with less training data and smaller model sizes. *ArXiv*, abs/2305.02301, 2023. URL <https://api.semanticscholar.org/CorpusID:258461606>. 3
- Edward J Hu, Yelong Shen, Phillip Wallis, Zeyuan Allen-Zhu, Yuanzhi Li, Shean Wang, Lu Wang, and Weizhu Chen. LoRA: Low-rank adaptation of large language models. In *International Conference on Learning Representations*, 2022. URL <https://openreview.net/forum?id=nZeVKeeFYf9>. 5.2
- Itay Itzhak and Omer Levy. Models in a spelling bee: Language models implicitly learn the character composition of tokens. In Marine Carpuat, Marie-Catherine de Marneffe, and Ivan Vladimir Meza Ruiz, editors, *Proceedings of the 2022 Conference of the North American Chapter of the Association for Computational Linguistics: Human Language Technologies*, pages 5061–5068, Seattle, United States, July 2022. Association for Computational Linguistics. doi: 10.18653/v1/2022.naacl-main.373. URL <https://aclanthology.org/2022.naacl-main.373>. 7
- Tom Leinster. How the simplex is a vector space. https://golem.ph.utexas.edu/category/2016/06/how_the_simplex_is_a_vector_sp.html, 2016. Accessed: 2024-03-12. 2
- Yi Liu, Gelei Deng, Yuekang Li, Kailong Wang, Tianwei Zhang, Yepang Liu, Haoyu Wang, Yanhong Zheng, and Yang Liu. Prompt injection attack against llm-integrated applications. *ArXiv*, abs/2306.05499, 2023. URL <https://api.semanticscholar.org/CorpusID:259129807>. 8
- John X. Morris, Wenting Zhao, Justin T Chiu, Vitaly Shmatikov, and Alexander M. Rush. Language model inversion. *ArXiv*, abs/2311.13647, 2023. 3, 6.3, 7
- Subhabrata Mukherjee and Ahmed Hassan Awadallah. Distilling transformers into simple neural networks with unlabeled transfer data. *ArXiv*, abs/1910.01769, 2019. URL <https://api.semanticscholar.org/CorpusID:203736526>. 3
- OpenAI, Josh Achiam, Steven Adler, Sandhini Agarwal, Lama Ahmad, Ilge Akkaya, Florencia Leoni Aleman, Diogo Almeida, Janko Altschmidt, Sam Altman, et al. Gpt-4 technical report, 2024. 1
- Mukul Singh, José Cambronero, Sumit Gulwani, Vu Le, Carina Negreanu, and Gust Verbruggen. Codefusion: A pre-trained diffusion model for code generation, 2023. 4

Florian Tramèr, Fan Zhang, Ari Juels, Michael K. Reiter, and Thomas Ristenpart. Stealing machine learning models via prediction apis. In *USENIX Security Symposium*, 2016. URL <https://api.semanticscholar.org/CorpusID:2984526>. 3.4

Ashish Vaswani, Noam M. Shazeer, Niki Parmar, Jakob Uszkoreit, Llion Jones, Aidan N. Gomez, Lukasz Kaiser, and Illia Polosukhin. Attention is all you need. In *Neural Information Processing Systems*, 2017. URL <https://api.semanticscholar.org/CorpusID:13756489>. 2

Zhilin Yang, Zihang Dai, Ruslan Salakhutdinov, and William W. Cohen. Breaking the softmax bottleneck: A high-rank RNN language model. In *ICLR*, 2018. URL <https://openreview.net/forum?id=HkwZSG-CZ>. 2

A Proofs

This appendix contains derivations for the equations used to solve for unbiased token probabilities given biased LLM outputs.

A.1 Fast logprobs algorithm

Our goal is to prove

$$p_i = \frac{p'_i}{\exp b_{\max} - \exp b_{\max} \sum_{j=1}^k p'_j + \sum_{j=1}^k p'_j} \quad (6)$$

Proof. We begin with the definition of the softmax function

$$p'_i = \frac{\exp(\ell_i + b_{\max})}{\sum_{j=1}^k \exp(\ell_j + b_{\max}) + \sum_{j=k+1}^v \exp \ell_j} \quad (7)$$

We then rearrange to obtain

$$\sum_{j=k+1}^v \exp \ell_j = \frac{\exp(\ell_i + b_{\max})}{p'_i} - \sum_{j=1}^k \exp(\ell_j + b_{\max}), \quad (8)$$

the lefthand side of which is independent of the bias term, meaning it is equivalent to when $b_{\max} = 0$, i.e.,

$$\frac{\exp \ell_i}{p_i} - \sum_{j=1}^k \exp \ell_j = \frac{\exp(\ell_i + b_{\max})}{p'_i} - \sum_{j=1}^k \exp(\ell_j + b_{\max}). \quad (9)$$

We can now rearrange

$$\frac{\exp \ell_i}{p_i} = \frac{\exp(\ell_i + b_{\max})}{p'_i} - \sum_{j=1}^k \exp(\ell_j + b_{\max}) + \sum_{j=1}^k \exp \ell_j \quad (10)$$

$$p_i = \frac{\exp \ell_i}{\frac{\exp(\ell_i + b_{\max})}{p'_i} - \sum_{j=1}^k \exp(\ell_j + b_{\max}) + \sum_{j=1}^k \exp \ell_j} \quad (11)$$

and expand

$$p_i = \frac{p'_i \exp \ell_i}{\exp(\ell_i + b_{\max}) - p'_i \sum_{j=1}^k \exp(\ell_j + b_{\max}) + p'_i \sum_{j=1}^k \exp \ell_j} \quad (12)$$

$$= \frac{p_i'^2 \exp(-b_{\max}) \exp(\ell_i + b_{\max})}{\exp(\ell_i + b_{\max}) - p'_i \sum_{j=1}^k \exp(\ell_j + b_{\max}) + p'_i \exp(-b_{\max}) \sum_{j=1}^k \exp(\ell_j + b_{\max})} \quad (13)$$

and finally simplify by multiplying the top and bottom of the right hand side by

$$\frac{1}{\sum_{j=1}^k \exp(\ell_j + b_{\max}) + \sum_{j=k+1}^v \exp \ell_j}$$

and which converts each term of the form $\exp(\ell_i + b_{\max})$ to p'_i , resulting in

$$p_i = \frac{p_i'^2 \exp(-b_{\max})}{p'_i - p'_i \sum_{j=1}^k p'_j + p'_i \exp(-b_{\max}) \sum_{j=1}^k p'_j} \quad (14)$$

$$= \frac{p'_i \exp(-b_{\max})}{1 - \sum_{j=1}^k p'_j + \exp(-b_{\max}) \sum_{j=1}^k p'_j} \quad (15)$$

$$= \frac{p'_i}{\exp b_{\max} - \exp b_{\max} \sum_{j=1}^k p'_j + \sum_{j=1}^k p'_j}, \quad (16)$$

which concludes the proof. \square

A.2 Numerically stable algorithm

The next proof is much simpler. Our goal is to prove

$$p_i = \exp(\log p'_i - b_{\max} - \log p'_v + \log p_v). \quad (17)$$

Proof. We begin with four facts

$$p_i = \frac{\exp \ell_i}{\sum_{j=1}^v \exp \ell_j} \quad p'_i = \frac{\exp \ell'_i}{\sum_{j=1}^v \exp \ell'_j} \quad p_v = \frac{\exp \ell_v}{\sum_{j=1}^v \exp \ell_j} \quad p'_v = \frac{\exp \ell'_v}{\sum_{j=1}^v \exp \ell'_j} \quad (18)$$

which follow from the definition of softmax. Combining these, we have

$$\frac{p_i}{\exp \ell_i} = \frac{p_v}{\exp \ell_v} \quad \text{and} \quad \frac{p'_i}{\exp \ell'_i} = \frac{p'_v}{\exp \ell'_v}. \quad (19)$$

Combining these again, we get

$$\frac{p_i}{p_v \exp \ell_i} = \frac{p'_i}{p'_v \exp \ell'_i}, \quad (20)$$

which we can rearrange to obtain

$$\frac{p'_v p_i}{p'_i p_v} = \frac{\exp \ell_i}{\exp \ell'_i}. \quad (21)$$

Next, we use the fact that $\exp \ell'_i = \exp b_{\max} \exp \ell$ to get

$$\frac{p'_v p_i}{p'_i p_v} = \exp(-b_{\max}). \quad (22)$$

which we can take the log of, rearrange, and exponentiate to achieve our goal

$$p_i = \exp(\log p'_i - b_{\max} - \log p'_v + \log p_v). \quad (23)$$

\square

A.3 Stochastically robust algorithm

We would like to derive

$$\log p_v - \log p_{v-1} = \log p'_v - \log p'_{v-1}. \quad (24)$$

Proof. Using our result from Appendix A.2, we have

$$p_i = \exp(\log p'_i - b_{\max} - \log p'_v + \log p_v) \quad (25)$$

$$p_i = \exp(\log p'_i - b_{\max} - \log p'_{v-1} + \log p_{v-1}). \quad (26)$$

Simply setting the righthand sides equal to one another, taking the log of both sides, then subtracting identical terms from both sides gives us our goal. \square